FREQUENCY BASED SUBSTRUCTURING WITHOUT R-DOF MEASUREMENTS: A TWO-BEAM TEST CASE

Emmanuel Pagnacco, Emmanuel.Pagnacco@insa-rouen.fr
Christophe Gautrelet, Christophe.Gautrelet@insa-rouen.fr
Jeremy Paumelle, Jeremy.Paumelle@insa-rouen.fr
Sylvain Lambert, Sylvain.Lambert@insa-rouen.fr
LMR – INSA de Rouen, BP 8, 76801 St. Etienne du Rouvray Cedex, France

Daniel J. Rixen, d.j.rixen@tudelft.nl
Delft UT, Faculty of Mechanics, Mekelweg 2, 2628 CD Delft, The Netherlands

Abstract. *When assembling measured frequency response functions (FRFs) of components to build an experimental model a major challenge consists in properly accounting rotational degrees-of-freedom (R-dofs) on the interface. Indeed the dynamic response of R-dofs are usually only known implicitly through the measurement of translations dofs. In theory using enough translational dofs for the interface coupling allows building accurate assembled models. In practice however even small errors in the measured FRFs will lead to huge inaccuracies in the assembled model, especially when stiff interfaces are considered. In this work, a solution is therefore described and tested on the assembly of two beams. In order to reduce the effect of measurement errors and enhance the coupling results several procedures are applied. In this paper, we will present the results for the coupling of two beams, using measured data and we will indicate how the proposed procedure can improve the coupled model significantly.*

Keywords*: Frequency Based Substructuring, Equivalent Multi-Point Connection, rotational degrees of freedom, stiff interface*

1. INTRODUCTION

Predicting system responses from coupled substructures is a very useful enterprise in mechanical manufacturing. In numerical analyses, dynamic substructuring methods are well established: dividing a system in subparts and assembling them on the interface enables handling each component independently in view of model reduction or parallel computing. It is highly desirable to have similar procedures to handle the experimental Frequency Response Functions (FRF) matrices, which characterise substructures. Indeed, coupling of FRF matrices of measured components, possibly with numerically modelled parts, allows us to include in the model complex substructures identified directly from dynamic measurements. Such a kind of assembly is called Frequency Based Substructuring (FBS).

Experimental FBS have become an important research issue in the last years (Jetmundsen 1986, Ewins 2003, Gonçalves de Lima and Rade 2005, De Klerk et al. 2006, Rixen et al. 2006, De Klerk et al. 2008…), since it offers several possibilities such as:

- to combine measured components or modelled and measured components to allow a rapid evaluation of the dynamics of the complete system ;
- to extract the dynamics of a components, having measured the dynamics of the complete system and of the others components. These procedures are also called “decoupling” (Ewins 2003) or “fictitious domains” (De Klerk *et al.* 2008).

However, to couple substructures, one must often account for the Rotational degrees of freedom (R-dofs) at the interface, similarly to interfaces finite element models of beams, plates and shells. But, in many practical situations, experimental components are known only by their translational FRF matrices (translational response over force). Moreover, data are generally noisy, which results in inaccuracies for the assembled system since the FRF matrices need to be inverted during the assembly process. When a numerical model of the components is available strategies such as SEREP can be used to recover the R-dofs by expending experimental data (Nicgorski 2008). However when no numerical model is available or when measurements are too noisy the assembly remains difficult. In this work, we use the Equivalent Multi-Point Connection (EMPC) method in order to tackle this difficulty.

The EMPC method is classically used in Finite Element Analysis (FEA) to couple subsystems having discrete dofs at their interfaces. Then, the interface consists of multiple points or nodes with multiple directions. This coupling strategy is employed here to assemble experimental components, by involving sufficient translational FRF along the interface to account for implicit rotational information (De Klerk *et al.* 2008). Thus, as the number of measurements points used in this kind of coupling corresponds to the number of DoF describing the interface, a minimum of 2 coupling DoF at two nodes are necessary to describe one translation and one rotation of a rigid interface. Let us note that whereas in FEA a point-wise connection guarantees compatibility along the interface since identical shape functions are assumed between the nodes, a point-wise connection of experimental FRFs implies that the compatibility is only enforced on those points, leaving the interface non-connected between the measured dofs. Taking into account more interface DoFs allows a richer description of the interface rigid motion, at least in a least-square sense.

This paper is organized as follows: section 2 describes the theory of the FBS and EMPC methods used here, including a filtration step using interface modes. The two beam test case is developed in section 3.

2. ELEMENTS OF THEORY

Let us consider the dynamic equation of motion of a component in the frequency domain:

$$\mathbf{Z}(\omega)^{(s)}\mathbf{U}(\omega)^{(s)} = \mathbf{F}(\omega)^{(s)} \tag{1}$$

In equation (1), $\mathbf{Z}^{(s)}$ represents the dynamic stiffness matrix of subsystem s while $\mathbf{U}^{(s)}$ and $\mathbf{F}^{(s)}$ represent the response and force vectors of the subsystem respectively. In this equation the force vector includes externally applied forces as well as interface internal forces. One has to note that this equation in the frequency domain can be written for different type of responses (*i.e.* displacement, velocity or acceleration) in which case the dynamic stiffness has a different physical meaning. Equation (1) is written here in displacement and can be rewritten as

$$\mathbf{U}(\omega)^{(s)} = \mathbf{Y}(\omega)^{(s)}\mathbf{F}(\omega)^{(s)} \tag{2}$$

where $\mathbf{Y}^{(s)}$, the inverse of the dynamic stiffness matrix $\mathbf{Z}^{(s)}$, is the so-called receptance matrix of subsystem s.

To couple subsystems, we introduce the Boolean Mapping Matrix $\mathbf{B}$ which contains information about the pairing of dofs on the interface. The compatibility condition imposing that the degrees of freedom on the interface have to be equal along the interface can be written as

$$\mathbf{B}\,\mathbf{U} = \mathbf{0} \tag{3}$$

In Lagrange Multiplier Frequency Based Substructuring (LM FBS), the matrix of the coupled system is assembled in a dual manner and the compatibility condition on the interface will be juxtaposed to the subsystem dynamic equilibrium equation (1). The internal interface forces, denoted by λ, enforce the compatibility constraints and the local dynamic equilibrium (1) can be written in block form as

$$\mathbf{Z}\,\mathbf{U} + \mathbf{B}^{\mathrm{T}}\lambda = \mathbf{F} \tag{4}$$

where we have used the block partitioned matrices (here explained for two substructures *a* and *b*)

$$\mathbf{Z} = \begin{bmatrix} \mathbf{Z}^{(a)} & \mathbf{0} \\ \mathbf{0} & \mathbf{Z}^{(b)} \end{bmatrix}, \qquad \mathbf{U} = \begin{bmatrix} \mathbf{U}^{(a)} \\ \mathbf{U}^{(b)} \end{bmatrix}, \qquad \mathbf{B} = \begin{bmatrix} \mathbf{B}^{(a)} & \mathbf{B}^{(b)} \end{bmatrix} \tag{5}$$

In equation (4) the operator $\mathbf{B}^{\mathrm{T}}$ defines on which DoFs the connecting forces will be applied, λ being the Lagrange multipliers associated to the constraints (3).

Combining the dynamic equilibrium equations (4) with the compatibility equations (3) the behaviour of the complete system can be described by

$$\begin{bmatrix} \mathbf{Z} & \mathbf{B}^{\mathrm{T}} \\ \mathbf{B} & \mathbf{0} \end{bmatrix} \begin{bmatrix} \mathbf{U} \\ \lambda \end{bmatrix} = \begin{bmatrix} \mathbf{F} \\ \mathbf{0} \end{bmatrix} \tag{6}$$

Solving the local equilibrium equations in (6) for λ, one finds

$$\mathbf{U} = \mathbf{Y}\left(\mathbf{F} - \mathbf{B}^{\mathrm{T}}\lambda\right) \tag{7}$$

where $\mathbf{Y} = \mathbf{Z}^{-1}$ (assuming that the receptance matrices of the substructures are not singular). Substituting in the second set of equations of (6) representing the compatibility equations, one obtains

$$\mathbf{B}\,\mathbf{Y}\,\mathbf{B}^{\mathrm{T}}\lambda = \mathbf{B}\,\mathbf{Y}\,\mathbf{F} \tag{8}$$

In practice, receptance matrices $\mathbf{Y}^{(s)}$ are composed of only discrete measurement points related to translational DoFs. Similarly to FEA these quantities are able to give correct interface flexibility when sufficient points are involved on the interface. Such a connection is called Equivalent Multi-Point Connection (EMPC) and this concept is applied here to the experimental coupling. But FEA results are free from noise, not experimental data. For that reason we introduce here the concept of EMPC with the Rigid Body Modes (RBM) filtration. Denoting $\mathbf{U}_c^{(s)}$ the coupling DoFs on the interface and $\mathbf{U}_i^{(s)}$ the internal DoFs of $\mathbf{U}^{(s)}$, we define

$$\mathbf{U}^{(s)} = \begin{bmatrix} \mathbf{U}_c^{(s)} \\ \mathbf{U}_i^{(s)} \end{bmatrix}, \qquad \mathbf{G} = \begin{bmatrix} \mathbf{R} & \mathbf{0} \\ \mathbf{0} & \mathbf{I} \end{bmatrix} \tag{9}$$

where the matrix $\mathbf{G}$ is a transformation matrix which will be used to represent the boundary behaviour in terms of interface modes $\mathbf{R}$ (subscript *s* is omitted in these matrices to simplify the notations). In the paper (and thus for the example of the two-bam assembly) we assume that it is sufficient to consider as interface flexibility modes the rigid modes on the interface. For instance, the $\mathbf{R}$ matrix is constituted by RBM to describe a rigid interface motion. Then, as explained in De Klerk *et al.* (2008), it is possible to reduce the FRF at the interface of a subsystem *s* while filtering out the noise measurements on these points by building the FRF related to the rigid interface modes as follows:

$$\tilde{\mathbf{Y}}_{\mathrm{R}}^{(s)} = \mathbf{T}\,\mathbf{Y}^{(s)}\,\mathbf{T}^{\mathrm{T}} \tag{10}$$

with

$$\mathbf{T} = \left(\mathbf{G}^{\mathrm{T}}\mathbf{G}\right)^{-1}\mathbf{G}^{\mathrm{T}} \tag{11}$$

However, we are interested in this work to keep the original measurement points as degrees of freedom in order to have more insight in results. Thus we have chosen to replace the original receptance matrix of subsystem *s* $\mathbf{Y}^{(s)}$ by its filtered counterpart $\tilde{\mathbf{Y}}^{(s)}$ which is define by

$$\tilde{\mathbf{Y}}^{(s)} = \mathbf{G}\,\mathbf{Y}_{\mathrm{R}}^{(s)}\,\mathbf{G}^{\mathrm{T}} \tag{12}$$

Since the number of interface modes in $\mathbf{G}$ is lower than the number of interface dofs, $\mathbf{G}\left(\mathbf{G}^{\mathrm{T}}\mathbf{G}\right)^{-1}\mathbf{G}^{\mathrm{T}} \neq \mathbf{I}$, and thus the transformation operator $\mathbf{T}$ acts as a spatial filter on the measured interface: it maps in a least square sense the interface dofs on the interface modes. Applying this step is especially necessary when the measurement errors are related to very stiff deformations, induced thus very high force errors. This is for instance true on a beam connection where many interface dofs are measured[1].

3. A TWO BEAMS TEST CASE

3.1. Presentation, measurements and numerical investigations

This section handles the case study of a two-beam assembly. Both beams are cantilevered and made out of steel (see Fig. 1). They have a length of 354 and 170 mm with a 5x39 mm^2 rectangular cross-section. The assembly is made by gluing side by side the two free extremities of the beams (along a 24mm long interface). Clamped supports are heavy and isolated from the outside world by viscoelastic supports. Measurements are performed with a VXI mainframe, an external piezo-electric sensor conditioner, a laser vibrometer and an automatic impacter equipped with a piezo-electric force sensor in order to obtain data as noiseless and accurate as possible (Gautrelet *et al.*, 2005).

Measurements points are only chosen along the interface. Including also transfer functions of internal dofs would not add any difficulties but would render the experiment more tedious. Hence, since no internal dofs are considered the matrix $\mathbf{G}$ involved in Eq. 7 is simply $\mathbf{R}$. We have retained five points to couple the beams, which are located on the middle of the height, every 5 mm. Since the displacements on the interface points was measured only in the transverse direction, a dataset of 25 FRFs for each substructure (5x5 matrices) is obtained. Measurement range goes from 0 to 1600 Hz with 401 spectral lines.

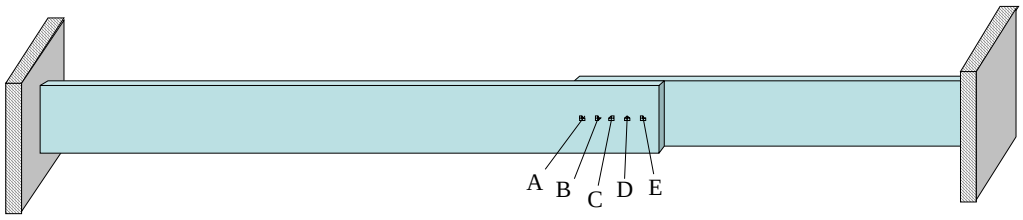

Figure 1. The test case of the two cantilever beams shown in the assembly configuration with measurements points

[1] Note that the concept used here can be interpreted as a SEREP method, but then without expansion and with RBM modes instead of FE modes.

First, it is verified that the measured FRFs of both single beams exhibit a behaviour very similar to what would be obtained from a numerical model (obtained from spectral finite elements) and one can also observe the very good reciprocity (*i.e.* measured FRFs matrices are really symmetric). Then, to ensure the validity of the test case defines, the FBS procedure is carrying out with these numerical FRFs, assembling only the translational DoFs of the sub-models. This allows checking that assembling the interface only through the displacements (namely letting the rotations free and non-assembled on those nodes) one obtains FRFs very similar to those obtained with full assembly on the nodes. Obviously omitting the R-dofs in the assembly is licit only for the first modes (low frequency range) where the interface deformation over the five nodes is mainly linear. This check is necessary to ensure that the assembly performed in the experimental FBS approach is licit.

Comparison of the numerical result with experimental FRF of the real assembly is very good, as shown in the Fig. 2 for two driving points (the first one, denoted C, being at the middle of the interface while the second one, denoted E, being at the interface extremity of the long beam). Driving points C and E are interesting to monitor since point C is located at the centre of the interface while point E is located on a vibration node of the fourth bending mode. One can see in figure 2 that the resonances related to the first five bending modes are well reproduces. Only one peak (at 660 Hz) is not found in the numerical assembly. A further investigation with the help of a more elaborate FE model has shown that this peak is associated to the first bending mode in the direction orthogonal to the measurement directions, and thus enters the assembled FRFs do to tiny cross-talk in the measurement pick-up. This peak will thus be disregarded in the following.

Table 1 gives the bending natural frequencies found for the two beams and their assembly. Additional measurements with an eccentricity location have been done also to identify frequencies of torsion modes. Only one additional frequency is found in the measurement range at 876 Hz for the two beams assembly. The associated peak is well decoupled from the others found on the mid of the height.

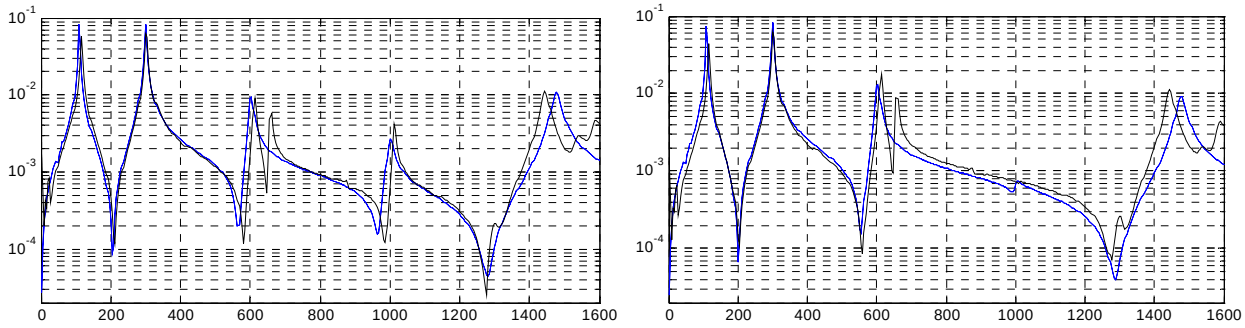

Figure 2. Comparison between numerical (blue) and experimental (black) FRF of the assembly at driving points C (left) and E (right).

Table 1. Experimental resonant frequencies of bending modes found in the 0-1600 Hz range for the two substructures and the assembly.

Mode	1st	2nd	3rd	4th	5th
Short beam	164	1016			
Long beam	34	216	602	1167	
Assembly	116	300	612	1012	1444

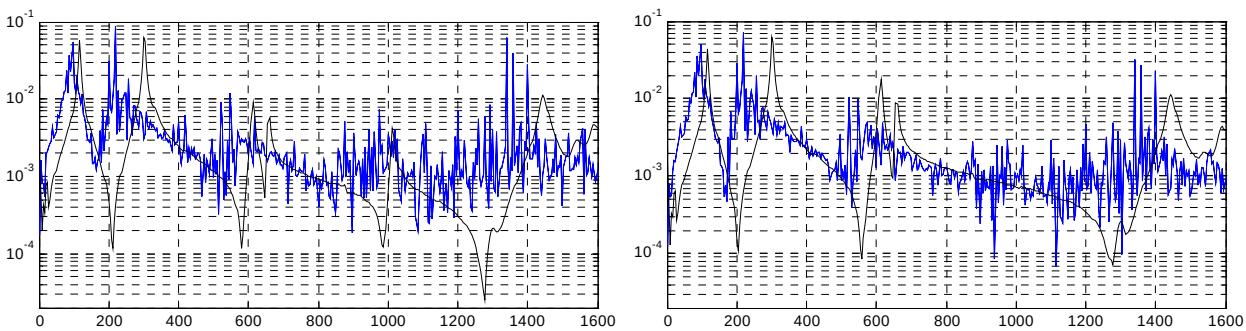

Figure 3. Assembly result with noisy numerical FRF (in blue) for 2 driving points C (left) and E (right). Experimental FRF are in black.

As a second step in the investigation, 0.5 % noise is added to numerical FRFs of single beams. This noise is added in the time domain. Results showed a catastrophic effect on the FRFs of the assembly (Fig. 3), with the first and second peak that are located now around 164 and 216 Hz. This indicates that adding random noise on the translation FRFs of points on a stiff interface can strongly pollute the assembly. Therefore, we suspect some difficulties when FBS will be applied to experimental data, even if they seem noise free. Such a result in presence of noise is not very surprising since a similar result was previously obtained in Ewins 2003 for a numerical investigation of the disassembly on a simple frame structure.

3.2. From very poor to satisfactory FBS results

A direct assembly of experimental data is carried out with the FBS strategy presented above. Unfortunately, with or without the application of the RBM-EMPC strategy, very bad results are obtained. Figure 4 presents the result without the use of the RBM-EMPC, but both results appear very similar. In these figures, one can see that the first and second peak are again located around 164 and 216 Hz (as predicted by the numerical tests with noise pollution).

Since RBM-EMPC is a spatial filter, the next idea is to combine this filter with a frequency filter to improve these results. Several strategies based on Singular Value Decomposition (SVD) with different threshold or different number of singular vectors have been tried, but without success[2]. Then, it was decided to investigate the assembly of synthesized FRF obtained through an experimental modal analysis of the substructures. Results found for the FBS were satisfactory in the range of 0-1100 Hz when using these synthesized FRF combined next with the RBM-EMPC strategy. This is shown in the figure 5, where discrepancies between FBS and assembly FRF are very small, with an exception for the first bending mode, which is subjected to a little shift of his peak. At contrary, unsatisfactory results are achieved by using only synthesized FRF without RBM-EMPC in FBS (Fig. 6). Although the combination of EMPC and modal synthesis in the FBS looks effective, this procedure will suffer of experimental modal analysis limitations (such as the modal truncation, which are unavoidable, as we can see in the figure 5 for the high frequency range).

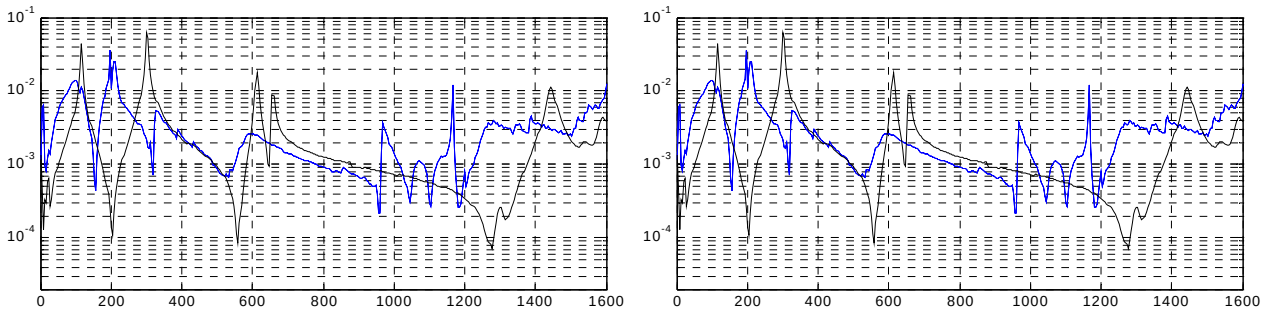

Figure 4. FBS results (blue) with original data for driving points C (left) and E (right).
Experimental FRF of the assembly are in black.

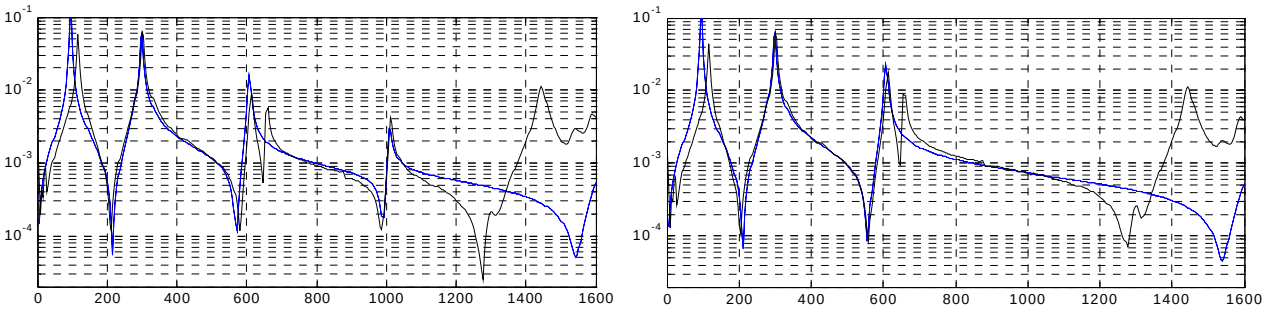

Figure 5. FBS results using modal synthesized FRF and RBM-EMPC (blue) for driving points C (left) and E (right).
Experimental FRF of the assembly are in black.

[2] Filtering FRF has been investigated in several manners. In a first attempt, we have determined principal components of the FRF data set via a SVD analysis and select the major principal components in order to exclude noise (Pickrel, 1995). In a second attempt, the singular values of the Hankel matrix formed by the impulse response function of the considered FRF are computed and a cut-off is chosen according to the number of modes of the studied substructure (Sanliturk and Cakar, 2005).

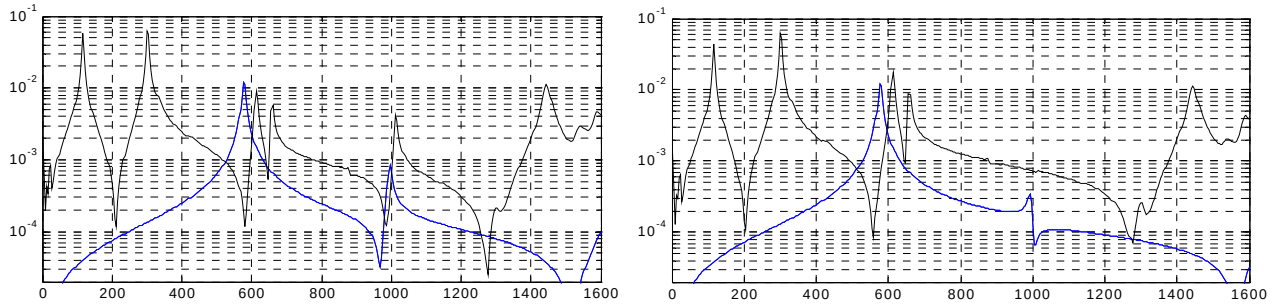

Figure 6. FBS results using synthesized FRF only (no RBM filter) (in blue) for driving points C (left) and E (right). Experimental FRF of the assembly are in black.

To understand more about FBS, we are coming back to the LM-FBS theory with experimental data. In LM-FBS, the $\tilde{\mathbf{Y}}_R$ matrix given by Eq. 11 gives an insight in the substructure FRF matrix involved in the coupling at the interface. Such a matrix has a dimension of 2X2 for each substructure, with the (1,1)[3] driving FRF is related to the rigid translation of the interface, whereas the (2,2) driving FRF characterizes the rotation of the interface segment. The $\tilde{\mathbf{Y}}_R$ FRF matrix obtained from the 5x5 experimental FRF matrix of the short beam is plotted against its modal synthesized counterpart in figure 7. If the FRF of the (1,1) driving point given by experimental data looks classical, with a good agreement with the synthesized one, this is not the case of the (2,2) FRF driving point. Indeed, one observes a severe disagreement with the synthesized FRF almost everywhere between resonant peaks. Same things could be noticed also for the long beam.

This clearly indicates that the raw FRF data measured on the interface are not sufficiently accurate to properly represent the rigid rotation of the interface, and only a modal identification can reveal the dynamic behaviour for the rotation.

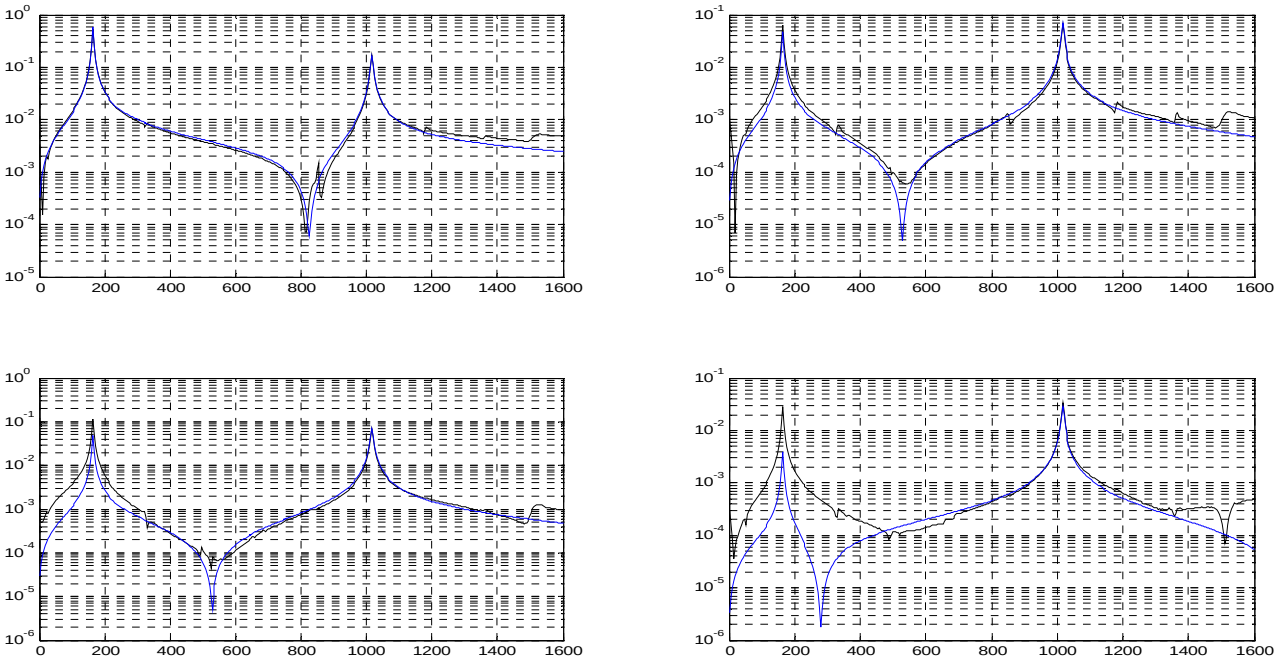

Figure 7. Projection of the experimental FRF matrix at the centre of the interface for the short beam (black), or by using synthesized FRF (blue).

3.3. Sensitivity analysis

In this subsection, we are interested in evaluating the sensitivity of the FBS method to some bias or noise in measurements for this two beams assembly. Conclusions or recommendations about measurements about FBS are expected from these sensitivities.

[3] The notation (*i*,*j*) used here stands for the *i*-th row, *j*-th column of the considered matrix.

3.3.1 Sensitivity to anti-resonance location

The sensitivity of the FBS to a shift for the anti-resonant frequency of the substructures is of interest. Indeed, many reasons (from testing to experimental modal analysis through measurements parameters) could lead to a disagreement in the anti-resonance location between the synthesized FRF used in the FBS and the "true" FRF. In Fig. 8 and 9, the shifts investigated are displayed. These two curves were obtained from measurements where small differences in parameters selection were introduced when performing the experimental modal analysis. In these 2 tests, synthesized FRF for the short beam are kept constant, while only synthesized FRF of the long beam differs. Fig. 8b and 9b displayed such differences on a typical FRF point, where the frequency of the anti-resonance located between the second and the third resonant peak is shifted. As a result, we can see that the shift introduce in the first test (Fig. 8) has a limited impact on the FBS, the main modification being on the frequency of the third peak. On the other end, the second test (Fig. 9) leads to catastrophic results for FBS, while the considered shift is only a little bit accentuated compared to the previous test.

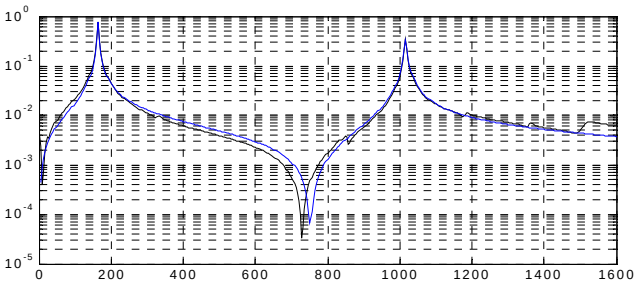

a) Synthesized FRF (blue) *vs.* experimental FRF for driving FRF on point A (short beam)

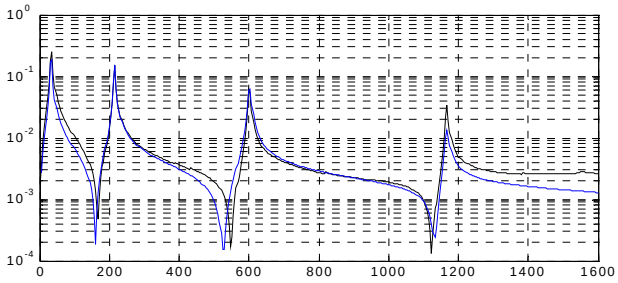

b) Synthesized FRF (blue) vs. experimental FRF for driving FRF on point A (long beam)

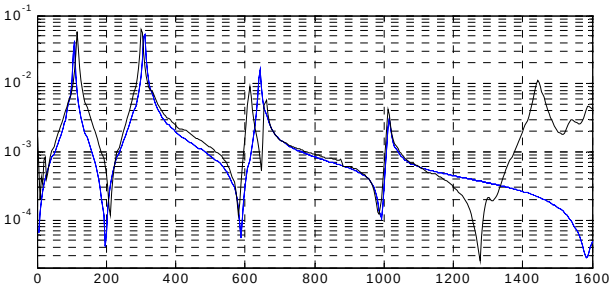

c) Assembly FRF of the driving point C

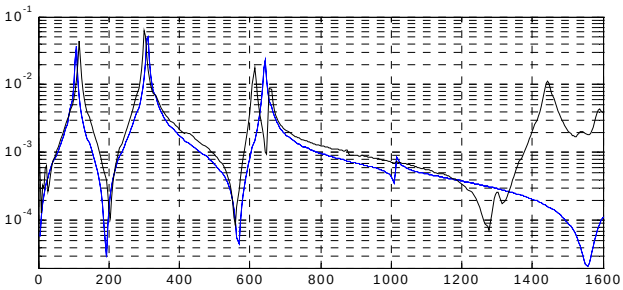

d) Assembly FRF of the driving point E

Figure 8. FBS with synthesized FRF having some frequency shift for anti-resonances and RBM-EMPC. Experimental FRF are in black.

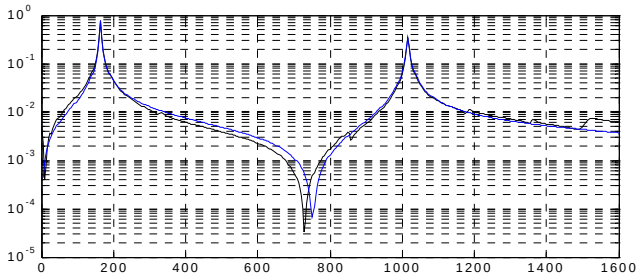

a) Synthesized FRF (blue) vs. experimental FRF for driving FRF on point A (short beam)

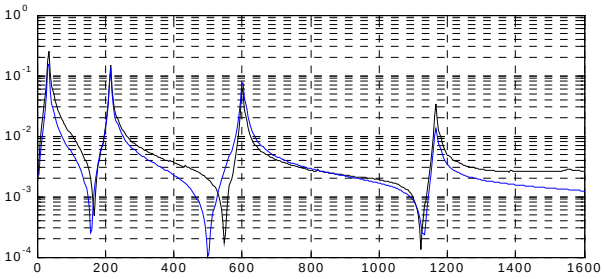

b) Synthesized FRF (blue) vs. experimental FRF for driving FRF on point A (long beam)

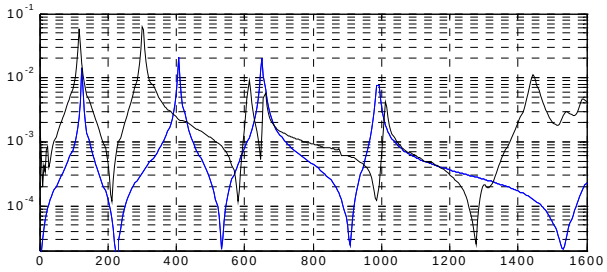

c) Assembly FRF of the driving point C

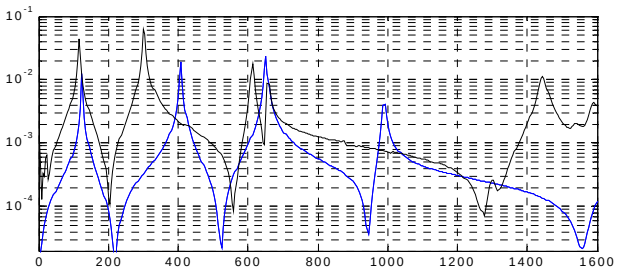

d) Assembly FRF of the driving point E

Figure 9. FBS with synthesized FRF having some more frequency shift for anti-resonances and RBM-EMPC. Experimental FRF are in black.

3.3.2 Sensitivity to the deepness of the anti-resonances

The sensitivity of the FBS to a bad amplitude evaluation of the anti-resonances in the FRF of substructures is of interest. Indeed, such a situation could occur depending of the instruments used for testing. For instance, we experience this situation when testing these beams using a spectrum analyzer having a built-in piezo-electric sensor conditioner. In figures 10a and 10b, such FRFs are displayed (in red) against the FRF currently acquired (in black). In these figures, the curve in blue shows the FRF modified by using the RBM-EMPC spatial filter. Results of the FBS are displayed in figure 10c and 10d and indicate a dramatic sensitivity to these anti-resonance bad definitions.

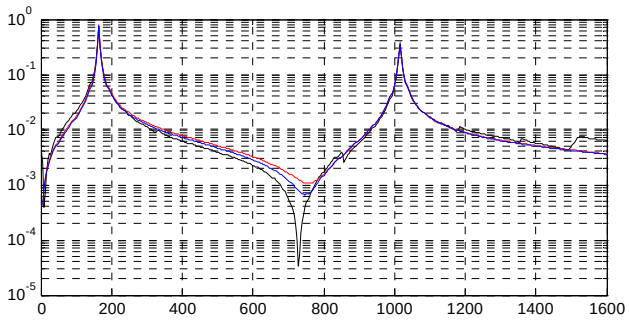

a) Synthesized FRF (blue) *vs.* experimental FRF for driving FRF on point A (short beam)

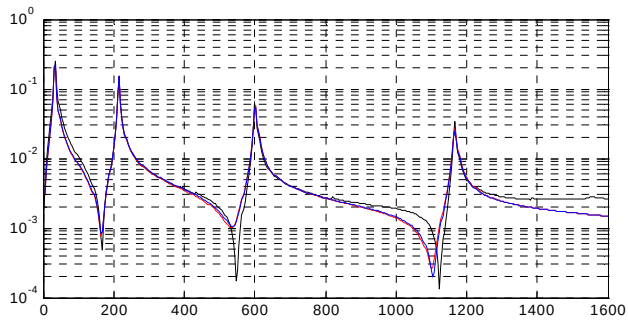

b) Synthesized FRF (blue) *vs.* experimental FRF for driving FRF on point A (long beam)

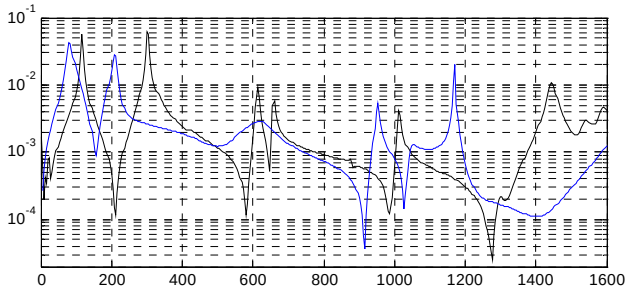

c) FBS for the driving point C

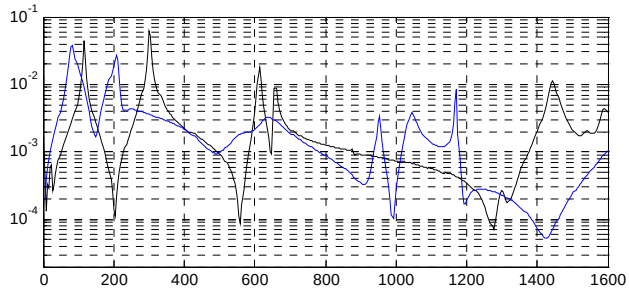

d) FBS for the driving point E

Figure 10. FBS with synthesized FRF having some bad definition for anti-resonances and RBM-EMPC. Experimental FRF are in black.

3.3.3 Modifying the number of coupling DoFs

Another interesting parameter of the experimental test concerns the number of chosen measurements points at the interface. Such a coupling is actually easy to evaluate for this test since it suffices to run the FBS procedure by deleting one rows and one column (or more) of the FRF matrices in order to discard one (or more) of the coupling nodes. We have investigated three cases where 4 nodes are kept, deleting successively either node B, C or D. Then we kept 3 nodes, deleting nodes B and D. Modal synthesis and RBM filter are enabled in these tests and it is seen that results with 3 coupling nodes are similar to others involving 4 coupling nodes. They are shown in the Fig. 11. In this figure, a shift for resonant peaks 2 and 3 is seen, and a disagreement for the anti-resonance located between these peaks is observed.

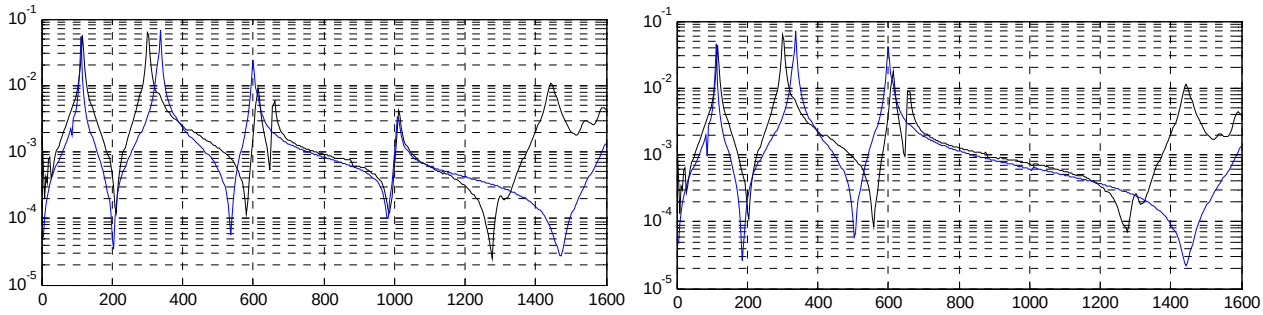

Figure 11. FBS with synthesized FRF and EMPC for 3 interface points. Experimental FRF are in black.

We thus conclude that coupling with less points decrease the quality of the FBS results and that 5 coupling points are necessary in this test in order for the RBM filtering in the EMPC to properly estimate the interface motion in a least square sense.

3.3.4 Further insights in the FBS method: using a 2 steps-LM FBS strategy

The LM FBS method is achieved now in two steps. The first one consists in evaluating the Lagrange multipliers, or, equivalently, the interface forces (eq. 8). The second one evaluates the assembly FRF by expressing the displacements from the substructure FRF and the Lagrange multipliers (eq.7). Since only the first step necessitates a matrix inversion, it is assumed to be the most sensitive to noise in the measurements, while the second steps won't be. To confirm this hypothesis, FBS is evaluated from the eq. 7 with the raw experimental FRFs, whereas the Lagrange multipliers are evaluated from modal synthesis FRF filtered with RBM-EMPC. Since DoFs of the assembly are replicated in eq. 7 (as many times as the number of the substructures), two results are displayed in the Fig. 12.

The two results indicate that peaks of resonant frequencies are recover, with some dummy peaks in addition. The analysis of these dummy peaks shows that their frequencies correspond exactly to the resonant frequencies of the substructure involved in the reconstruction (given by the eq. 7). Then, the assembled FRF obtained with the FRF of the short beam exhibit a dummy peak around 164 Hz between the first and the second resonant peak of the assembly, while the assembly FRF obtained with the FRF of the long beam exhibit two dummy peaks around 34 and 216 Hz in the 0-300 Hz range. Thus, it is concluded that the resonances of the substructures involved in the assembly lead to dummy peaks at these frequencies in the FBS result. This observation gives certainly an explanation of peaks that appears in Figure 3 and 4. These effects have been further explained in Rixen 2008.

Moreover, we have obtained the same findings even if the EMPC strategy is carried out in the FBS second step. Such results could constitute an explanation for the bad FBS results when using the original data (fig. 4) with only the RBM-EMPC spatial filter (*i.e.* without the modal filtering). Further investigations show that the RBM-EMPC spatial filter is really needed only for the determination of the Lagrange multipliers.

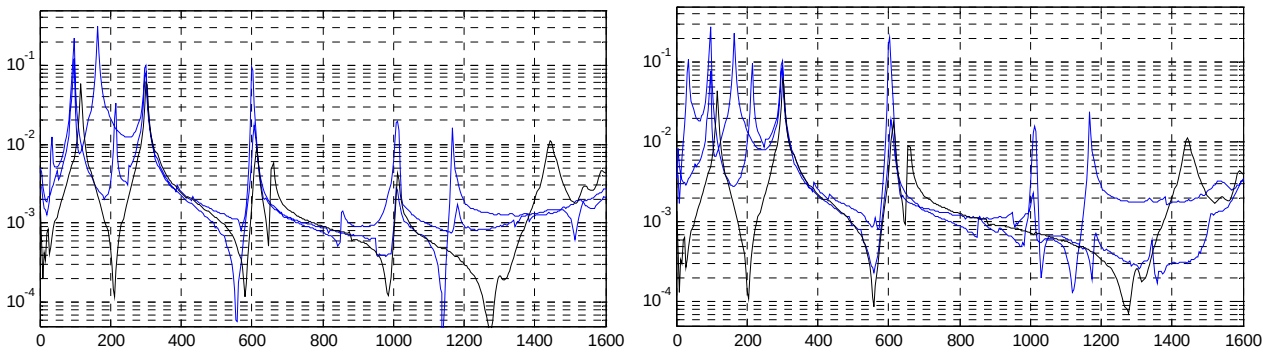

Figure 12. FBS with synthesized FRF and EMPC for the interface force evaluation only
Experimental FRF are in black.

4. CONCLUSIONS

In this work, we have studied the coupling of experimental substructures when R-Dofs responses are not available, taking as case study the assembly of two cantilevered beams. *A priori*, the basic FBS (without modal synthesis) is the most interesting approach since it avoids errors that could be introduced by an experimental modal analysis. The main ingredients for a successful FBS, *i.e.* an FBS not too sensitive to noise measurements and which handle the lack of R-DoFs data, are a dual assembly, which keeps the number of inversion with experimental data as small as possible, with an equivalent multi-point connection which is constrained to follow a rigid body motion along the interface.

The first step to validate this strategy was done by correlating numerical data -involving only T-DoFs- to experimental ones for each substructure and for the measured full assembly. The results form the FBS assembly were very bad due to even small measurement errors. SVD filtering strategies did not help. In order to obtain good FBS results we have used FRFs synthesized from an experimental modal analysis of substructure data, followed by a spatial projection in the subspace spanned by rigid body modes. Having to resort to modal synthesis is not a joyful prospective since it renders the technique more cumbersome, but it helps here to conduct a sensitivities study on this basic example.

We have observed a high sensitivity of the FBS results to bias measurements, such as a bad location or a bad amplitude of the anti-resonance in the FRF. Such sensitivity is logical, since each frequency point of the FRF is affected in its level between two resonant frequencies if the anti-resonant frequency is not well located. On the other hand, we have been surprised by the high sensitivity of the coupling to anti-resonance frequencies, since a small shift on these parameters could lead to catastrophic results.

We thus conclude that extreme care must be taken during the measurements to ensure an accurate identification of these anti-resonances (choice of instruments and amplifiers). And this is again true if experimental modal analysis is used to couple substructures. However, a benefit of RBM-EMPC is the capacity to relocate (to some extent) the anti-resonant frequencies. But this capacity is certainly linked to the number of measurements points on the interface (a least-square procedure is involved here to filtered out the measurement noise).

Finally, we have also found that dummy peaks in the assembly could come from the resonant peaks of substructures. Moreover, such dummy peaks appear easily, when expressing responses from substructures FRF and interface forces. On the other hand, they are easy to identify from substructures FRF.

5. REFERENCES

De Klerk, D., Rixen, D.J., Voormeeren, S.N., 2008, “General Framework for Dynamic Substructuring: History, Review and Classification of Techniques”, AIAA Journal., vol. 46, no. 5, pp. 1169-1181.

De Klerk, D., Rixen, D.J., Voormeeren, S.N., Pasteuning, F., 2008, “Solving the RDoF Problem in Experimental Dynamic Substructuring”, Proceedings of the IMAC-XXVII Conference, Orlando, Florida USA, 9 p.

Ewins, D.J., 2003, “Impedance Based Decoupling and its Application to Indirect Model Testing and Component Measurement: A Numerical Investigation”, Proc. of the IMAC-XXI conference, Kissimmee, Florida USA, 7 p.

Gautrelet, C., Pagnacco, E., Moreau, A., Borza, D., Lemosse, D., 2005, “Mesure de champ pour l’identification de propriétés élastiques et viscoélastiques”, Proceedings of “Sixième colloque international francophone – MTOI”, Marseille, France, 6 p.

Gonçalves de Lima, A.M., Alves Rade, D., 2005 , “Modelling of Structures Supported on Viscoelastic Mounts Using FRF Substructuring”, International Conference on Sound and Vibration, ICSV12, Lisboa, Portugal, 9 p.

Jetmundsen, B., “On Frequency Domain Methodologies for Structural Modification and Subsystem Synthesis”, Ph.D. thesis, Rensselaer Polytechnic Institute, Troy, NY, 1986.

Nicgorski D., Avitabile P., 2008, “Conditioning of frf measurements for use with frequency based substrucuring”, Proceedings of the IMAC-XXVII Conference, Orlando, Florida USA.

Pickrel, R. C, 1995, “Estimating the Rank of Measured Response Data Using SVD and Principal Response Functions”, Proc DTA NAFEMS conference on Model Updating, Scotland, pp 89-99.

Rixen, D.J., Godeby, T., Pagnacco, E., 2006, “Dual Assembly of substructures and the FBS Method: Application to the Dynamic Testing of a Guitar”, Proceedings of the ISMA Conference, Leuven, Belgium, 15 p.

Rixen, D.J., 2008, “How measurement inaccuracies induce spurious peaks in Frequency Based Substructuring”, Proceedings of the IMAC XXVII Conference, Orlando, Florida USA.

Sanliturk, K. Y.; Cakar, O., 2005, “Noise elimination from measured frequency response functions”, Mechanical Systems and Signal Processing, Volume 19, Issue 3, p. 615-631.

6. RESPONSIBILITY NOTICE

The authors are the only responsible for the printed material included in this paper.